Memorandum 001

Epoch-Dependent Dispersion and Scattering along Pulsar Lines of Sight

J.M. Cordes

2014 November 28

http://nanograv.org/

Epoch-Dependent Dispersion and Scattering along Pulsar Lines of Sight

J. M. Cordes

Apr 11 – November 28, 2014, v1.71

Contents

1 Introduction

In these notes, epoch and frequency-dependent effects from interstellar refraction and diffraction are analyzed. Three calculations are described. The first considers changes in DM due solely to motions of the pulsar and the solar system through interstellar gas. The second analyzes the apparent frequency dependence of the dispersion measure (DM) caused by the strong variation of the scattered image with frequency. The third concerns the effects of a refracting screen on measurable quantities such as arrival time, scintillation parameters, and scattered images and pulse shapes.

For some cases, the combined effects of interplanetary and interstellar propagation are important. Discussion of these is deferred to another analysis.

Dispersion and scattering are assumed to result from cold plasma in the high-frequency limit with negligible contributions from magnetic fields.

The first calculation is based on a medium having an arbitrary electron density distribution and only considers dispersion. The results include identification of both systematic and random contributions to DM. These effects need to be combined with refraction and scattering for a complete discussion of chromatic timing variations (which are considered in the third calculation).

In the second calculation (§3), a thin plasma screen transverse to the pulsar direction has electron density variations are described by a power-law wavenumber spectrum extending over a wide range of wavenumbers. Angular broadening introduces an averaging length scale in the medium that causes the dispersion measure (DM) to vary with frequency. The essential effect is that DM at a frequency ν' random walks away from DM at frequency ν as the ratio ν/ν' gets larger.

In the third calculation (§4), a thin screen is again used to analyze the interplay of dispersion, refraction, and diffraction and flux-density variations by assuming that refraction and diffraction arise from very different length scales so that they can be separated mathematically. This approach differs significantly from the second calculation but is motivated by long-standing evidence that the interstellar medium is more complex than an idealized power-law wavenumber spectral description.

In various places, specific pulsars are mentioned and specific studies are suggested for developing a better understanding of the importance of various effects and understanding the ISM. Timing

precision is the ultimate driver of these studies and follow-on studies for timing precision will be described elsewhere.

It is expected that the results from all three calculations will need to be considered together in a global analysis. Specific modeling of lines of sight can make use of scintillation-arc studies (e.g. Stinebring 2007) that help locate electron-density enhancement along specific lines of sight.

2 DM Variations from Pulsar and Solar System Motion

Summary of this section: The dispersion measure will vary with time due to motions of the pulsar and observer (and in some cases the medium) both along the line of sight (LOS) and transverse to the LOS. Figure 1 shows the geometry. The LOS at $t = 0$ and $t > 0$ will differ by parallel and perpendicular vectors,

$$\boldsymbol{\ell}_{\parallel}(t) = \Delta\mathbf{v}_{\parallel} t \equiv (\mathbf{v}_{e_{\parallel}} - \mathbf{v}_{p_{\parallel}})t, \quad (1)$$

$$\boldsymbol{\ell}_{\perp}(t, z) = \mathbf{v}_{\mathrm{eff}_{\perp}}(z)t, \quad (2)$$

where $\mathbf{v}_{\mathrm{eff}_{\perp}}(z)$ is the effective velocity at each location z along the LOS (defined below in Eq. 9).

Comments:

- The parallel and perpendicular offsets are comparable in magnitude (statistically).
- $\mathrm{DM_t}$ will vary with time from parallel motion alone regardless of whether the ISM is uniform or not; no gradients in electron density n_e are needed. The variations will be monotonically increasing or decreasing with time if there is no transverse motion (of the pulsar, solar system, or medium).
- DM variations from transverse motion alone require gradients in n_e that have components transverse to the LOS, i.e. $\nabla n_e \cdot \boldsymbol{\ell}_{\perp} \neq 0$.
- Any gradients in n_e will generally be manifested from both parallel and transverse motion.
- DM variations from parallel motion do not depend on the pulsar distance but the transverse change in LOS depends on location along the LOS, therefore influencing the observable effect from a transverse gradient.
- When the Earth's orbital velocity is important, such as for a millisecond pulsar with low translational velocity, the contribution to $\mathrm{DM_t}$ depends on $\nabla n_e \cdot \mathbf{v}_{\mathrm{eff}_{\perp}}(z, t)$ and therefore will show a sinusoidal variation.

A useful form for $\mathrm{DM_t}$ is

$$\boxed{\mathrm{DM_t} = \mathrm{DM_0} + \left[\mathrm{n_e}(\mathbf{x}_{\mathrm{p0}})\mathrm{v}_{\mathrm{p}_{\parallel}} - \mathrm{n_e}(\mathbf{x}_{\mathrm{e0}})\mathrm{v}_{\mathrm{e}_{\parallel}}\right]\mathrm{t} + \int_{\mathrm{z_{e_0}}}^{\mathrm{z_{p_0}}} \mathrm{dz}\,\Delta\mathrm{n_e}(\mathbf{x}_{\mathrm{t}}(\mathrm{z})).} \quad (3)$$

The first term is the value at $t = 0$. The second term arises from parallel motion for the case where there are no strong gradients in n_e that are encountered over time t at either the pulsar location ($\mathbf{x}_{p_0}$) or near the solar system ($\mathbf{x}_{e_0}$). This term by itself produces a DM structure function that is

quadratic. The third term involves variations in n_e on scales of order the change in LOS over time t. For a stochastic medium, such as one with a Kolmogorov spectrum, this term gives the standard $\propto t^{5/3}$ scaling. However, small clouds with sizes of tens of AU and larger will also produce a quadratic structure function. Investigation of DM variations therefore needs to account for these square-law effects before the structure function can be interpreted in terms of any kind of power-law wavenumber spectrum.

Some interesting implications of these results are:

1. Some pulsars will show $\mathrm{DM_t}$ variations where parallel motion is more important than transverse motion, and vice versa.
2. The two kinds of variations may be distinguishable. If gradients and transverse motion are dominant, there should also be epoch-dependent refraction and flux-density variations on the same time scales. However, parallel-motion effects need not be accompanied by strong modulations of scintillation parameters and flux densities.
3. ISM structure local to the solar system may contribute to $\mathrm{DM_t}$ variations and they will be partially correlated between different pulsars. Representative numbers suggest that this effect is likely very small, at least at the present epoch. An upper bound may provide useful constraints on the local ISM and heliospheric boundary.

2.1 Basic Setup

Consider changes in DM that result from motions of the pulsar and observer, which change both the distance to the pulsar and the direction of the LOS, as shown in Figure 1. The initial distance $D_0 = |\mathbf{x}_{p0} - \mathbf{x}_{e0}|$ increases (to first order in time) as

$$D(t) \approx D_0 + (\mathbf{v}_p - \mathbf{v}_e) \cdot \hat{\mathbf{n}}_0 \, t \equiv D_0 + \Delta v_\parallel t. \tag{4}$$

The next, quadratic term, $(\Delta v_\perp t)^2/2D_0$, is $\Delta v_\perp t/D_0 \sim 10^{-6}$ times smaller than the linear term for typical parameters (100 km s^{-1} velocity, 10-yr time span, and 1 kpc distance) and therefore can be ignored in calculating the distance. The change in the unit vector toward the pulsar is determined by the transverse velocity

$$\hat{\mathbf{n}}_t = \hat{\mathbf{n}}_0 + D_0^{-1} \Delta \mathbf{v}_\perp t, \tag{5}$$

where $\hat{\mathbf{n}}_0 = \Delta \mathbf{x}_0 / D_0 = (\mathbf{x}_{p0} - \mathbf{x}_{e0})/D_0$.

Let the initial LOS at $t = 0$ be the z-axis and integrate over locations $\mathbf{x}_0(z) = z\hat{\mathbf{z}}$ to get

$$\mathrm{DM_0} = \int_{\mathrm{z_{e_0}}}^{\mathrm{z_{p_0}}} \mathrm{dz\, n_e}(\mathbf{x}_0(\mathrm{z}). \tag{6}$$

For $t > 0$ we integrate over a new interval $[z_e, z_p]$ where

$$z_e = z_{e_0} + v_{e_\parallel} \, t, \quad z_p = v_{p_\parallel} \, t. \tag{7}$$

The sampled locations are now $\mathbf{x}_t(z) = \mathbf{r}(z,t) + z\hat{\mathbf{z}}$ where $\mathbf{r}(z,t)$ is transverse to $\hat{\mathbf{z}}$,

$$\mathbf{r}(z,t) = \mathbf{v}_{\mathrm{eff}_\perp}(z) t \tag{8}$$

$$\mathbf{v}_{\mathrm{eff}_\perp}(z) = \mathbf{v}_{e_\perp} + (\mathbf{v}_{p_\perp} - \mathbf{v}_{e_\perp}) \left(\frac{z - z_e}{z_p - z_e} \right). \tag{9}$$

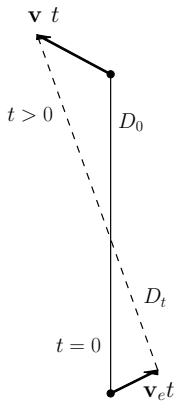

Figure 1: Geometry showing change in line of sight due to motion of pulsar and observer. DM is calculated by integrated along the z axis taking into account the change in LOS.

Note that the locations z_e and z_p are evaluated at time t and it is assumed that there is no significant acceleration correction over times of interest (years to decades).

The simplest approach is to evaluate the electron density for the $t > 0$ LOS in terms of its values for the initial line of sight,

$$\begin{aligned} n_e(\mathbf{x}_t(z)) &= n_e(\mathbf{x}_0(z)) + [n_e(\mathbf{x}_t(z)) - n_e(\mathbf{x}_0(z))] && (10) \\ &\equiv n_e(\mathbf{x}_0(z)) + \Delta n_e(\mathbf{x}_t(z)). && (11) \end{aligned}$$

The DM integral over $[z_e, z_p]$ can be expanded into a set of integrals over the three intervals $[z_{e_0}, z_p]$, $[z_{e_0}, z_e]$, and $[z_{p_0}, z_p]$ (Figure 2) to get

$$\begin{aligned} \mathrm{DM_t} &= \int_{z_e}^{z_p} dz\, n_e(\mathbf{x}_t(z)) && (12) \\ &= \int_{z_{e_0}}^{z_{p0}} dz\, n_e(\mathbf{x}_t(z)) + \int_{z_{p_0}}^{z_p} dz\, n_e(\mathbf{x}_t(z)) - \int_{z_{e_0}}^{z_e} dz\, n_e(\mathbf{x}_t(z)). && (13) \end{aligned}$$

For the first integral we expand the integrand using Eq. 11 to get

$$\int_{z_{e_0}}^{z_{p_0}} dz\, n_e(\mathbf{x}_t(z)) = \mathrm{DM_0} + \int_{\mathrm{z_{e_0}}}^{\mathrm{z_{p0}}} \mathrm{dz}\, \Delta \mathrm{n_e}(\mathbf{x}_\mathrm{t}(\mathrm{z})). \tag{14}$$

This gives

$$\boxed{\mathrm{DM_t} - \mathrm{DM_0} = \int_{\mathrm{z_{e_0}}}^{\mathrm{z_{p0}}} \mathrm{dz}\, \Delta \mathrm{n_e}(\mathbf{x}_\mathrm{t}(\mathrm{z})) + \int_{\mathrm{z_{p_0}}}^{\mathrm{z_p}} \mathrm{dz}\, \mathrm{n_e}(\mathbf{x}_\mathrm{t}(\mathrm{z})) - \int_{\mathrm{z_{e_0}}}^{\mathrm{z_e}} \mathrm{dz}\, \mathrm{n_e}(\mathbf{x}_\mathrm{t}(\mathrm{z})).} \tag{15}$$

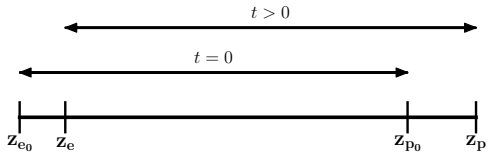

Figure 2: Three intervals along the z axis for calculating $\mathrm{DM_0}$ and $\mathrm{DM_t}$.

The first of these integrals involving $\Delta n_e(\mathbf{x}_t(z))$ needs to be considered only if electron density variations are significant on length scales of order the offset between the LOS at t and the initial LOS at $t = 0$, i.e. $|\Delta\mathbf{x}_t(z)| = |\mathbf{x}_t(z) - \mathbf{x}_0(z)| \ll D_0$, e.g. $\ell \sim 20$ AU $V_{\mathrm{eff}_\perp 100} t_{\mathrm{yr}}$ for a fiducial velocity of 100 km s^{-1} and a year-long time span. All evidence from the last few decades of interstellar scintillation studies are consistent with there being variations on these (multiples of AU) and smaller scales. However, the detailed spectrum of variations on AU scales is not well known and appears to differ between LOS to different pulsars.

The second two integrals in Eq. 15 are over small intervals $z_p - z_{p_0} = v_{p_\parallel} t$ and $z_e - z_{e_0} = v_{e_\parallel} t$ so, to first order in these intervals, the two terms give $\overline{n}_e(\overline{\mathbf{x}}_p) v_{p_\parallel} t$ and $\overline{n}_e(\overline{\mathbf{x}}_e) v_{e_\parallel} t$, where $\overline{n}_e(\overline{\mathbf{x}}_p)$ and $\overline{n}_e(\overline{\mathbf{x}}_e)$ are averages over the respective intervals centered on $\overline{\mathbf{x}}_p = \mathbf{x}_{p_0} + (v_{p_\parallel} t/2)\hat{\mathbf{n}}_t$ and $\overline{\mathbf{x}}_e = \mathbf{x}_{e_0} + (v_{e_\parallel} t/2)\hat{\mathbf{n}}_t$, respectively. Unless there are large variations over the intervals, these average locations can be taken as the initial ones at $t = 0$. The DM variations from these two terms are a simple consequence of the change in pulsar distance due to parallel motion (the transverse velocities enter only to second order and so are negligible in these terms).

When calculating the time derivative of $\mathrm{DM(t)}$ below, we will assume that true *temporal* changes in electron density are negligible. This is often a good assumption because turbulent ISM velocities are typically much smaller than pulsar velocities. For slow pulsars and fast plasma screens (e.g. shock fronts), the ISM velocity needs to be included. This modifies the effective velocity defined in Eq. 9 by adding $-\mathbf{v}_m(z)$ (with m for medium), as in Cordes & Rickett (1998). For a purely turbulent medium, this velocity is stochastic and would depend on wavenumber. However, a moving screen is easily described with a translational velocity.

2.2 Uniform Electron Density

For a perfectly uniform medium with density n_e the difference $\Delta n_e(\mathbf{x}_t(z))$ vanishes and the total DM is

$$\mathrm{DM_t} = \mathrm{DM_0} + \mathrm{n_e}(\mathrm{v_{p_\parallel}} - \mathrm{v_{e_\parallel}})\mathrm{t} \quad \text{(uniform medium)} \tag{16}$$

and its time derivative is

$$\frac{d\mathrm{DM}}{dt} = n_e(v_{p_\parallel} - v_{e_\parallel}). \tag{17}$$

For a constant electron density, $d\mathrm{DM}/\mathrm{dt}$ is proportion to the parallel velocity difference. An estimate of $d\mathrm{DM}/\mathrm{dt}$ assuming a fiducial relative velocity of 100 km s^{-1} and an ionized gas density of 0.1 cm^{-3} is

$$\frac{d\mathrm{DM}}{dt} \approx 10^{-5}\, v_{100} n_{e_{0.1}}\ \mathrm{pc\ cm^{-3}\ yr^{-1}} \tag{18}$$

2.3 Electron Density Variations on Large Length Scales

For a medium with changes in density only on large length scales $\gg |v_{p_\parallel} - v_{e_\parallel}|t$, the derivative still depends only on parallel velocities,

$$\frac{d\mathrm{DM}}{dt} = n_e(\mathbf{x}_{p_0})v_{p_\parallel} - n_e(\mathbf{x}_{e_0})v_{e_\parallel}. \tag{19}$$

Eq. 19 indicates that changes in DM are affected by the electron density on both ends of the LOS. For similar electron densities, we expect the pulsar term to dominate because pulsar velocities are typically much larger than the Earth's orbital motion and the Sun's peculiar motion relative to the Local Interstellar Cloud (LIC), about 23 km s^{-1}. There will be exceptions, of course, for pulsars with low velocities or with small parallel velocity components. The Earth's orbital motion is not relevant for this calculation because the Earth resides inside the heliosphere. However, if we include the interplanetary medium in the analysis (either explicitly here or separately as an additional non-ISM term), the Earth's velocity will of course matter.

The Earth term raises the interesting possibility that DM variations are partially correlated between different lines of sight with an angular dependence that depends on the local ISM and on the direction of the Sun's peculiar velocity. The heliospheric wake is estimated to be $\sim 10^3$ AU long and with a density $\lesssim 0.05$ cm^{-3} (Frisch 2007) that could provide $\delta\mathrm{DM} \sim$ multiples of 10^{-4} pc cm^{-3} in some directions.

The motion of the Sun through the local interstellar cloud (LIC) may be particularly interesting. The relative motion of the Sun and LIC is about 23 km s^{-1} based on measurements from the *Interplanetary Background Explorer* (IBEX) mission. The LIC is about 9.2 pc across and has an internal gas density of 0.3 cm^{-3} at a temperature of 6000 K. Assuming complete ionization, the total DM through the cloud is $\mathrm{DM_{LIC}} \approx 3$ pc cm^{-3} and the maximum derivative is

$$\frac{d\mathrm{DM}}{dt} \approx 0.7 \times 10^{-5}\ \mathrm{pc\ cm^{-3}\ yr^{-1}}. \tag{20}$$

2.4 Large and Small Electron Density Variations

Because the ionized ISM contains a wide range of length scales, the term in Eq. 15 involving $\Delta n_e(\mathbf{x}_t)$ also needs to be considered. Its contribution to DM is

$$\delta \mathrm{DM_t} = \int_{\mathrm{z_{e_0}}}^{\mathrm{z_{P0}}} \mathrm{dz}\, \Delta \mathrm{n_e}(\mathbf{x}_\mathrm{t}(\mathrm{z})). \tag{21}$$

Typical scales transverse to the LOS are $|\mathbf{r}| \sim v_\perp t \sim 20\ \mathrm{AU}\, v_{\perp 100} t_{\mathrm{yr}}$. The relevant velocity $\mathbf{v}_{\mathrm{eff}_\perp}(z)$ is largest at the pulsar position (c.f. Eq. 9) for cases where the proper-motion velocity is larger than the Earth's velocity. Elsewhere along the line of sight and for slowly moving millisecond pulsars, the transverse scale can be substantially smaller.

DM varies according to

$$\boxed{\mathrm{DM_t} = \mathrm{DM_0} + \left[\mathrm{n_e}(\mathbf{x}_{\mathrm{p_0}})\mathrm{v}_{\mathrm{p}_\parallel} - \mathrm{n_e}(\mathbf{x}_{\mathrm{e_0}})\mathrm{v}_{\mathrm{e}_\parallel}\right] \mathrm{t} + \int_{\mathrm{z_{e_0}}}^{\mathrm{z_{P0}}} \mathrm{dz}\, \Delta \mathrm{n_e}(\mathbf{x}_\mathrm{t}(\mathrm{z})).} \tag{22}$$

Linear trends in $\mathrm{DM_t}$ have been recognized for many years and it is not *a priori* obvious whether they should be associated with the explictly linear term in Eq. 22 or with the third term, which may quantify gradients transverse to the line of sight.

2.4.1 Structure Function of DM

The DM structure function,

$$D_{\delta \mathrm{DM}}(\tau) = \left\langle [\mathrm{DM_{t+\tau}} - \mathrm{DM_t}]^2 \right\rangle, \tag{23}$$

includes the effects of the systematic DM term due to the change in distance as well as the term involving the integrated difference $\Delta n_e(\mathbf{x}_t)$. Discrete structures on AU scales can contribute to $\Delta n_e(\mathbf{x}_t)$ (see below). Together, these and the changing distance will produce contributions to the structure function that are quadratic in τ. For the case where only the distance-change term is relevant, $\mathrm{DM_{t+\tau}} - \mathrm{DM_t} \propto \tau$, it is easy to show that the structure function is

$$D_{\delta \mathrm{DM}}(\tau) = \left[n_e(\mathbf{x}_{p_0}) v_{p_\parallel} - n_e(\mathbf{x}_{e_0}) v_{e_\parallel}\right]^2 \tau^2. \tag{24}$$

A general feature of structure functions is that they are quadratic when the lag τ is smaller than any characteristic time scale in the time series. So for structures in the ISM with scale sizes ℓ of tens of AU that have characteristic crossing times $\ell/\mathrm{V_{eff}} \sim$ many years, quadratic structure functions will be seen for lags of a few years or less.

For cases where the systematic term is significant, the time series for DM could be de-trended before calculating the structure function. Kolmogorov fluctuations will produce a non-quadratic scaling for the structure function $\propto t^{5/3}$ and will scale differently for other slopes of the electron density wavenumber spectrum as long as the spectral index $\beta < 4$ (as defined below). Equivalent to other discussions in the literature, when a power-law wavenumber spectrum dominates electron-density variations the structure function is essentially the structure function of $\delta \mathrm{DM_t}$ given in Eq. 21.

2.4.2 Discrete Structures

There is evidence for individual structures in the ISM on AU scales based on refraction effects in pulsar dynamic spectra, extreme scattering events, and intraday variable sources. These are likely confined to a small fraction of the LOS and will produce maximum contributions to DM of order $10^{-5} n_e \ell_{\rm AU}$ pc cm^{-3} where $\ell_{\rm 10AU}$ is the path length through the structure. The time scale for changes depends on the density, size, and velocity of the structure so the derivative $d{\rm DM}/{\rm dt}$ can be comparable to or much smaller or larger than the contribution from the changing distance analyzed in the previous subsection.

Clumps: Consider a single ionized cloud that has scales $a_\parallel$ and $a_\perp$ parallel and transverse to the LOS and with a column density ${\rm DM_c} = {\rm N_{e_c}}$ through the cloud along the LOS. The maximum phase change due to the clump is $\phi_c \sim \lambda r_e N_{e_c}$ and the dispersion delay is

$$\Delta t_{{\rm DM}c} = \frac{\phi_c}{2\pi\nu} = \frac{\lambda^2 r_e N_{e_c}}{2\pi c}. \tag{25}$$

The phase gradient across the LOS is then $|\nabla_\perp \phi| \sim \lambda r_e N_{e_c}/a_\perp$ and the refraction angle is

$$\theta_{r_c} = \frac{\lambda |\nabla_\perp \phi|}{2\pi} \sim \frac{\lambda^2 r_e N_{e_c}}{2\pi a_\perp} \sim \frac{c \Delta t_{{\rm DM}c}}{a_\perp}. \tag{26}$$

There are two time delays introduced by refraction into barycentric arrival times. The first is associated with the translation of topocentric TOAs by the propagation delay from the geocenter to the solar system barycenter. The direction to the pulsar is a key part of the translation. Chromatic refraction causes the angle of arrival to differ from an assumed direction, implying a delay (Foster & Cordes 1990) that varies sinusoidally with an annual period and an amplitude

$$\Delta t_{{\rm bary}_c} \sim \frac{r_\oplus \theta_r}{c} \sim \left(\frac{r_\oplus}{a_\perp}\right) \Delta t_{{\rm DM}c} \sim \frac{\Delta t_{{\rm DM}c}}{a_{\perp {\rm AU}}}, \tag{27}$$

where $r_\oplus = 1$ AU. The second delay is the geometric increase in propagation path that is roughly

$$\Delta t_{{\rm geo}_c} \sim \frac{D\theta_r^2}{2c} \sim \frac{cD(\Delta t_{{\rm DM}c})^2}{2{a_\perp}^2} \sim \frac{cD(\Delta t_{{\rm DM}c})^2}{2r_\oplus^2} \left(\frac{\Delta t_{{\rm DM}c}}{a_{\perp {\rm AU}}}\right)^2. \tag{28}$$

For a single clump, Eqs. 27 and 28 indicate that $\Delta t_{{\rm bary}_c}$ and $\Delta t_{{\rm geo}_c}$ are linear and quadratic, respectively, in the dispersion delay, $\Delta t_{{\rm DM}c}$. The scaling laws in these equations are consistent with those that can be derived from a more exact analysis of a Gaussian plasma lens (Clegg et al. 1998). The barycentric and geometric delays are comparable for pulsars within about 1 kpc because $\theta_r \sim 1$ mas and $D\theta_r \sim 1$ AU, though there are wide variations of these values.

Numerically, the refraction and dispersion delays are comparable for nominal parameter values but any one of the three can dominate the the other two for reasonable distances and transverse scale lengths,

$$\Delta t_{{\rm bary}_c} \sim 1\ \mu s \left(\frac{\Delta t_{{\rm DM}c,\mu s}}{a_{\perp {\rm AU}}}\right), \tag{29}$$

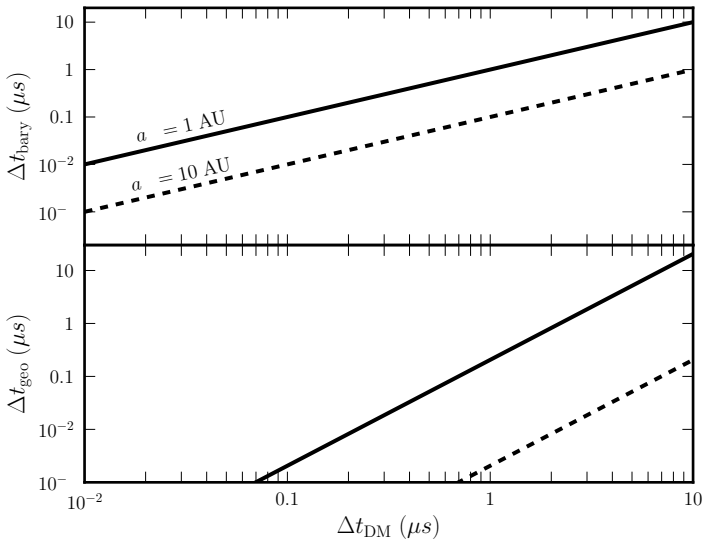

Figure 3: Refraction delays plotted against DM delay from a single cloud. (Top) The barycentric delay for two clump scale sizes, as labeled. (Bottom) The geometric delay for the same two clump sizes.

and

$$\Delta t_{\mathrm{geo}_c} \sim 0.2\ \mu s\, D_{\rm kpc} \left(\frac{\Delta t_{\mathrm{DM}c,\mu s}}{a_{\perp \mathrm{AU}}} \right)^2 . \tag{30}$$

Figure 3 shows $\Delta t_{\mathrm{bary}_c}$ and $\Delta t_{\mathrm{geo}_c}$ plotted against $\Delta t_{\mathrm{DM}c}$ for $D = 1$ kpc and for two transverse scale lengths ($a_\perp = 1$ and 10 AU).

A final consideration is multiple imaging. Clegg et al. (1998) analyze flux variations and caustics for a Gaussian lens. The focal distance $D_{\rm f}$ of a clump is the minimum distance from the clump at which rays can cross,

$$D_{\rm f} \sim \frac{a_\perp}{\theta_{r_c}} \sim \frac{{a_\perp}^2}{c \Delta t_{\mathrm{DM}c}} \sim 2.4\ \mathrm{kpc}\ {a_\perp}^2_{\rm AU} \Delta t_{\mathrm{DM}c,\mu s}. \tag{31}$$

We therefore do not expect ray crossing and multiple images from nearby pulsars unless a clump is small and dense.

Wedges: (Backer et al. 1993) proposed that plasma wedges are responsible for linear trends in $\mathrm{DM(t)}$. A plasma wedge has linearly increasing column density $N_e(\mathbf{x})$ transverse to the LOS. As the line of sight moves across it, $\mathrm{DM(t)}$ will change linearly until the wedge boundary is reached, if there is one. The wedge will also refract by a constant refraction angle. Unlike other structures, however, a wedge of this type will have zero transverse second derivative (except at the boundaries) and therefore will not cause changes in measured flux density.

Electron-density slabs: $\mathrm{DM(t)}$ time series from pulsars show a combination of linear trends, stochastic variations, and, in a few cases, fast changes in slope that are both positive and negative. Apparent slope changes can appear in particular realizations of a stochastic process with a

red power spectrum. But they can also result from slab-like structures if they are suitably oriented relative to the LOS and the pulsar's velocity. Such slabs may represent static increases and deficits over the local mean electron density that contribute as the LOS of changes with time. Alternatively, they could be time-dependent owing to shock motions through neutral gas. Bow shocks produced by the pulsars themselves may ionize atomic (and, less likely, molecular) structures as they move through the ISM.

So far, the cases considered have assumed that ISM structures are static. However, the pulsar can actively modify its local environment. An extreme case is where the pulsar's motion toward the observer takes it through *atomic* hydrogen (HI) structures on scales of tens of AU and larger, including filaments, (e.g. Stanimirović et al. 2007; Gibson 2007; McClure-Griffiths et al. 2007). As the pulsar nears a filament, it will ionize the atomic gas through a combination of radiation from the neutron star and magnetosphere and shock heating. The standoff radius of the bow shock is given by balance of ram pressure and the pulsar's relativistic wind,

$$r_s = \left(\frac{\dot{E}}{4\pi \rho v_p^2 c} \right)^{1/2} \approx 266 \text{ AU } \dot{E}_{33}^{1/2} n_H^{-1/2} v_{p100}^{-1} \tag{32}$$

for $\dot{E} = 10^{33} \dot{E}_{33}$ erg s^{-1}, a pulsar velocity in units of 100 km s^{-1}, and an effective hydrogen density n_H cm^{-3}. For the ranges of pulsar velocities, energy-loss rates ($\dot{E}$) and ISM densities, the standoff radius of the bow shock is tens of AU to ~ 0.1 pc. Therefore, $DM(t)$ can show temporary increases even though the prevailing trend would be a decrease because of the decreasing distance.

The effects of different geometries include:

Transverse motion ($v_{p_\parallel} = 0$): For a density enhancement that is aligned with the LOS, $\mathrm{DM_{slab}}(t)$ will consist of a positive-going 'pulse' with duration equal to the pulsar travel time across the slab thickness. For a density deficit (e.g. from encountering a slab of atomic gas), the pulse will be negative going. Figure 4 shows examples of $\mathrm{DM(t)}$ for transverse motion and an interleaved sequence of three density deficits and two enhancements that produce a train of pulses in $\mathrm{DM(t)}$. To first order, the pulsar distance does not change so the unperturbed DM is constant in time. slab with long dimension along the LOS:

Pulsar velocity component along the LOS ($v_{p_\parallel} \neq 0$) and aligned slabs: When the density slabs are aligned with the LOS, $DM(t)$ again show square-wave type pulses. Figure 5 shows $\mathrm{DM(t)}$ for a case where the pulsar travels through the slabs and another where it does not. The prevailing trend is for $DM(t)$ to decrease as the pulsar distance gets smaller, but this is interrupted by the density deficits and enhancements.

Pulsar velocity component along the LOS ($v_{p_\parallel} \neq 0$) and slanted slabs: When the density slabs are slanted from the LOS, $DM(t)$ can show a saw-tooth pattern where it has a larger slope than the prevailing trend or a slope with opposite sign. Figure 6 shows $\mathrm{DM(t)}$ for a case where the pulsar travels through the slabs and another where it does not. As with Figure 5, the prevailing trend is for $DM(t)$ to decrease as the pulsar distance gets smaller, but this is interrupted by the density deficits and enhancements.

Pulsar velocity toward the observer ($v_{p_\perp} = 0$): Figure 7 shows a case where the pulsar ionizes atomic hydrogen (blue boxes) as it passes into the box and schematically shows

Figure 4: Schematic change in dispersion measure due to line of sight sampling of interleaved electron-density deficits (white boxes) and enhancements (blue boxes). These cases are for pure transverse motion of the pulsar for which there is no prevailing trend of $DM(t)$. (Left) Density slabs aligned with the line of sight. (Right) Density slabs at an angle of 30° from the LOS.

Figure 5: Schematic change in dispersion measure due to line of sight sampling of interleaved electron-density deficits and enhancements. These cases are for pulsar motion with a component toward the observer (i.e. 80° from the LOS direction). The prevailing trend is for $\mathrm{DM(t)}$ to get smaller with time. (Left) Pulsar motion through the density slabs. (Right) Density slabs far from both observer and pulsar.

how increases in DM can occur even if the pulsar moves toward the observer and the prevailing trend is for a declining DM.

2.4.3 Spectrum of Electron-Density Variations

Consider a Kolmogorov-like spectrum of the form

$$P_{\delta n_e}(\mathbf{q}) = \mathrm{C_n^2}\ \mathrm{q}^{-\beta}, \qquad \mathrm{q_0} \leq \mathrm{q} \leq \mathrm{q_1} \tag{33}$$

where the scattering irregularities are isotropic and the spectrum depends only on the magnitude of the wavenumber. Evidence exists for anisotropic scattering but the analysis is accordingly more

Figure 6: Schematic change in dispersion measure due to line of sight sampling of interleaved electron-density deficits and enhancements. These cases are for pulsar motion with a component toward the observer (i.e. 80° from the LOS direction) and with slanted density slabs. The prevailing trend is for $\mathrm{DM(t)}$ to get smaller with time. (Left) Pulsar motion through the density slabs. (Right) Density slabs far from both observer and pulsar.

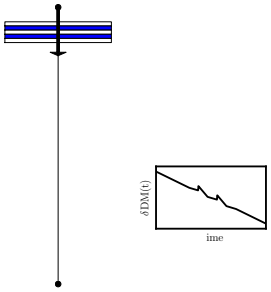

Figure 7: Motion of pulsar along line of sight toward observer. In this case, white boxes are density deficits while blue boxes represent density enhancements of atomic hydrogen that is ionized if the pulsar is in the box. The prevailing trend is for $\mathrm{DM(t)}$ to get smaller with time.

tedious. The Kolmogorov case corresponds to $\beta = 11/3$. For $\beta > 3$ and $q_0 \ll q_1$, the rms electron density is dominated by the largest scales. Defining the inner and outer scales (i.e. the smallest and largest scales) as ℓ_1 and ℓ_0, the wavenumber cutoffs are $q_0 = 2\pi/\ell_0$ and $q_1 = 2\pi/\ell_1$. For $\ell_1 \ll \ell_0$ and using a Kolmogorov spectrum, the rms electron density is

$$n_{e_{\rm rms}} \approx [3(2\pi)^{1/3}]^{1/2} \left(C_{\rm n}^2\right)^{1/2} \ell_0^{1/3}. \tag{34}$$

While the ISM seems to be described by outer scales that are quite large ($\sim$ 1 to 100 pc except in dense, compact regions), for the calculation here we use a scale of order the separation of the lines of sight over times up to 10 yr (e.g. tens of AU or less). Using $\mathrm{C_n^2} = 10^{-3.5}$ m$^{-20/3}$ as a typical value in the vicinity of the Sun and a fiducial scale $\ell_0 = 1$ AU, the rms electron density is

$$n_{e_{\rm rms}} \approx 2.2 \times 10^{-4}\ {\rm cm}^{-3}\ \ell_{0,\rm AU}^{1/3} \mathrm{C}^2_{\mathrm{n}_{-3.5}}. \tag{35}$$

By comparison, an outer scale of $L = 1$ pc yields $n_{e_{\rm rms}} \approx 0.013$ cm^{-3}.

For an extended medium, the number of independent fluctuations along the LOS at a given scale is $N(\ell) \approx \eta D/\ell$, where η is the LOS filling factor. For the warm ionized medium, the filling factor is estimated to be $\eta \sim 0.1$ to 0.2. The integrated δn_e is a random walk with $N(\ell)$ steps, yielding a sum that has a total rms value

$$n_{e_{\rm rms}}^{\rm total} = N^{1/2}(\ell) n_{e_{\rm rms}}(\ell) \propto (\eta D {\rm C}_{\rm n}^2)^{1/2} \ell_0^{-1/6}. \tag{36}$$

The corresponding DM variation is

$$\delta{\rm DM} = {\rm n}_{\rm e_{rms}}^{\rm total} \ell_0 \propto (\eta {\rm D C}_{\rm n}^2)^{1/2} \ell_0^{5/6}, \tag{37}$$

which is largest for larger scales ℓ_0. Estimated values for ${\rm C}_{\rm n}^2$ in the literature are based on LOS averages, so they already incorporate the filling factor We then can make the replacement ${\rm SM} = \eta {\rm D C}_{\rm n}^2$. The relevant scales are those that correspond to the transverse separation of the LOS at times $t = 0$ and $t > 0$. This separation varies along the line of sight but it is useful to consider a typical value. As discussed below, scattering causes any single-epoch measurement of DM to result from spatial averaging over the ISM. For the value of ${\rm C}_{\rm n}^2$ considered above and for a kpc distance, a typical scattering angle ~ 1 mas corresponds to a ~ 1 AU smoothing scale. This implies that the smallest scales will be averaged over[1] sufficiently to not contribute less than otherwise to significant variations of DM with epoch. The relevant scales are then expected to be ~ 1 to 10 AU and for a kpc distance and AU scales, we have

$$\delta{\rm DM} = 1.6 \times 10^{-5} \ {\rm pc \ cm^{-3}} \ \left({\rm D_{kpc} C}_{\rm n_{-3.5}}^2 \right)^{1/2} \ell_{0,{\rm AU}}^{5/6}. \tag{38}$$

We therefore expect the random component of ${\rm DM_t}$ to grow with time $\propto t^{5/6}$ because the LOS separation grows linearly with t. This is consistent with expressions for the DM structure function, whose square root scales as $t^{5/6}$.

The DM structure function from the random component in Eq. 21 is, for an arbitrary wavenumber spectrum,

$$D_{\delta{\rm DM}}(\tau) = 2 \int_{z_{e_0}}^{z_{p_0}} dz \int d\mathbf{q}_\perp \, P_{\delta n_e}(\mathbf{q}_\perp, q_z = 0, z) \left(1 - e^{i \mathbf{q}_\perp \cdot \mathbf{v}_{{\rm eff}_\perp}(z) \tau} \right). \tag{39}$$

For an isotropic wavenumber spectrum, this becomes

$$D_{\delta{\rm DM}}(\tau) = 4\pi \int_{z_{e_0}}^{z_{p_0}} dz \int dq_\perp q_\perp \, P_{\delta n_e}(q_\perp, q_z = 0, z) \left[1 - J_0(q_\perp V_{{\rm eff}_\perp}(z) \tau) \right]. \tag{40}$$

and for the power-law wavenumber spectrum of Eq. 33,

$$\boxed{D_{\delta{\rm DM}}(\tau) = 8\pi^2 f_\beta \int_{z_{e_0}}^{z_{p_0}} dz \, {\rm C}_{\rm n}^2({\rm z}) \left[{\rm V}_{{\rm eff}_\perp}({\rm z}) \tau \right]^{\beta - 2}} \tag{41}$$

[1]Note that 'averaging' is the correct term here, rather than summing, because the effects of scattering can be described as angular averaging using a function with unit area.

where (Cordes & Rickett 1998, Eq. B6)

$$f_\beta = \frac{8\pi^2}{(\beta-2)2^{\beta-2}} \frac{\Gamma(2-\beta/2)}{\Gamma(\beta/2)}. \tag{42}$$

The numerical factor is $f_{11/3} = 88.3$ for a Kolmogorov wavenumber spectrum with $\beta = 11/3$

Details of derivation:

The DM difference $\mathrm{DM_t} - \mathrm{DM_0}$ given by Eq. 21 has a mean-square value that is the structure function for a lag $\tau = t$ because we assume that stationary statistics apply. Using $\Delta n_e(\mathbf{x}_t(z))$ defined in Eq. 11, the mean-square is

$$\left\langle (\delta \mathrm{DM_t})^2 \right\rangle = \iint\limits_{z_{e_0}}^{z_{p_0}} dz\, dz'\, \langle \Delta n_e(\mathbf{x}_t(z)) \Delta n_e(\mathbf{x}_t(z')).\rangle \tag{43}$$

Expanding the integrand and taking into account that the mean electron density subtracts out, there are four terms, the most general one being

$$I = \iint\limits_{z_{e_0}}^{z_{p_0}} dz\, dz'\, \langle \delta n_e(\mathbf{x}_t(z)) \delta n_e(\mathbf{x}_0(z'))\rangle\,, \tag{44}$$

The integrand depends on only the spatial difference

$$\delta \mathbf{x}_t(z,z') \quad = \quad \mathbf{x}_t(z)) - \mathbf{x}_0(z') = (z-z')\hat{\mathbf{z}} + \mathbf{v}_{\mathrm{eff}_\perp}(z)t. \tag{45}$$

Changing variables to $z_+ = z + z'/2$ and $z_- = z - z'$ this becomes

$$\delta \mathbf{x}_t(z,z') = z_- \hat{\mathbf{z}} + \mathbf{v}_{\mathrm{eff}_\perp}(z_+ + z_-/2)t. \tag{46}$$

Writing the autocorrelation function $R_{\delta n_e}(\delta \mathbf{x})$ of $\delta n_e(\mathbf{x})$ in terms of the wavenumber spectrum,

$$R_{\delta n_e}(\delta \mathbf{x}) = \int d\mathbf{q}\, P_{\delta n_e}(\mathbf{q}) e^{i\mathbf{q}\cdot\delta\mathbf{x}}, \tag{47}$$

we have, using $D_0 = z_{p_0} - z_{e_0}$,

$$I_t = \int_{z_{e_0}}^{z_{p_0}} dz_+ \int_{-D_0}^{D_0} dz_- \int d\mathbf{q}\, P_{\delta n_e}(\mathbf{q}) e^{i\mathbf{q}\cdot[z_-\hat{\mathbf{z}} + \mathbf{v}_{\mathrm{eff}_\perp}(z_+ + z_-/2)t]} \tag{48}$$

The integral over z_- is over a range that is twice the distance to the pulsar, which we assume exceeds the outer scale of the wavenumber spectrum by many orders of magnitude. This yields to good approximation a delta function

$$\begin{aligned} &\int_{-D_0}^{D_0} dz_-\, e^{i\mathbf{q}\cdot[z_-\hat{\mathbf{z}} + \mathbf{v}_{\mathrm{eff}_\perp}(z_+ + z_-/2)t]} \\ &\qquad = \delta(q_z + \mathbf{q}_\perp \cdot \Delta\mathbf{v}_\perp t/2(z_p - z_e)) e^{i\mathbf{q}_\perp \cdot \mathbf{v}_{\mathrm{eff}_\perp}(z_+)t}. \end{aligned} \tag{49}$$

Integrating over q_z then yields

$$I_t \quad = \quad \int_{z_{e_0}}^{z_{p_0}} dz_+ \int d\mathbf{q}_\perp\, P_{\delta n_e}(\mathbf{q}_\perp, q_z = -\mathbf{q}_\perp \cdot \Delta\mathbf{v}_\perp t/2(z_p - z_e)) e^{i\mathbf{q}_\perp \cdot \mathbf{v}_{\mathrm{eff}_\perp}(z_+)t}. \tag{50}$$

The integral can be simplified further by recognizing that the q_z argument of $P_{\delta n_e}(\mathbf{q}_\perp, q_z)$ is much smaller than $|\mathbf{q}_\perp|$ by roughly a factor of 10^{-7}, so we set $q_z = 0$ and get

$$I_t \quad = \quad \int_{z_{e_0}}^{z_{p_0}} dz_+ \int d\mathbf{q}_\perp \, P_{\delta n_e}(\mathbf{q}_\perp, 0) e^{i\mathbf{q}_\perp \cdot \mathbf{v}_{\mathrm{eff}_\perp}(z_+)t}. \tag{51}$$

The structure function is then twice the difference between I_0 and I_t,

$$\left\langle (\delta \mathrm{DM_t})^2 \right\rangle = 2(I_0 - I_t) = 2 \int_{z_{e_0}}^{z_{p_0}} dz_+ \int d\mathbf{q}_\perp \, P_{\delta n_e}(\mathbf{q}_\perp, 0) \left[1 - e^{i\mathbf{q}_\perp \cdot \mathbf{v}_{\mathrm{eff}_\perp}(z_+)t} \right]. \tag{52}$$

When the wavenumber spectrum describes isotropic irregularities, we use $d\mathbf{q}_\perp = d\phi \, dq_\perp \, q_\perp$ and allow the spectrum to be variable along the LOS on scales larger than the outer scale to get

$$\left\langle (\delta \mathrm{DM_t})^2 \right\rangle = 2 \int_{z_{e_0}}^{z_{p_0}} dz_+ \int dq_\perp \, q_\perp P_{\delta n_e}(q_\perp, 0, z_+) \left[1 - J_0(q_\perp V_{\mathrm{eff}_\perp}(z_+)t) \right]. \tag{53}$$

For the power-law spectrum of Eq. 33, this becomes

$$\left\langle (\delta \mathrm{DM_t})^2 \right\rangle = 4\pi \int_{z_{e_0}}^{z_{p_0}} dz_+ \, \mathrm{C_n^2(z_+)} \int_{\mathrm{q_0}}^{\mathrm{q_1}} \mathrm{dq_\perp \, {q_\perp}^{1-\beta}} \left[1 - \mathrm{J_0(q_\perp V_{eff_\perp}(z_+)t)} \right]. \tag{54}$$

For offsets $2\pi/q_0 \ll V_{\mathrm{eff}_\perp}(z_+)t \ll 2\pi/q_1$, the wavenumber integral gives the standard scaling $\propto [V_{\mathrm{eff}_\perp}(z_+)t]^{\beta-2}$. The full expression for this regime is given in Eq. 41.

2.5 Published DM Variations: A Quick Summary and Suggested Analyses

Published time series of DM in the literature show several types of behavior. Some show linear trends with superposed correlated variations, while others show only correlated variations without an obvious trend. A few show piecewise linear variations that signify change points in the time derivative $d\mathrm{DM}/\mathrm{dt}$ associated with structure in the ISM on scales of 1-100 AU.

Interpretation of DM time series involves:

1. DM time series will generally include linear trends along with stochastic variations from density variations on a wide range of scales (e.g. Kolmogorov-like variations). Before using $\mathrm{DM(t)}$ to infer the properties of stochastic variations, the trends need to be removed. If they are not, the DM structure function will be contaminated by a square-law component that will cause the spectral index of the wavenumber spectrum (β) to be overestimated.
2. Estimates of DM will be contaminated by other chromatic timing effects that result from refraction and multipath propagation. As shown by (Foster & Cordes 1990), if refraction is allowed to contaminate DM estimates, the structure function will show excess amplitude on long times compared to extrapolation from the diffraction time scale and will also lead to an overestimated wavenumber spectral index.
3. Disentangling the effects of changing distance and changing line of sight from parallel and transverse motion, respectively, is possible if scintillation parameters (including flux density) are also measured. The change in distance over a few years will have no effect on these parameters whereas transverse gradients will.

B1937+21: The DM time series shows a long-term trend. Ilyasov et al. (2005) and Ramachandran et al. (2006) show a 20-year time series extending to $\sim$ 2003.5 (MJD 52800) that has a strong

decreasing trend with an average derivative $d\mathrm{DM}/\mathrm{dt} \approx -1.14 \pm 0.03 \times 10^{-3}$ pc cm^{-3} yr^{-1}. Long-term correlated variations are superposed with this trend.

B1821−24: Cognard & Lestrade (1997, see also Backer et al. (1993)) show a DM time series with a long-term increasing trend with $d\mathrm{DM}/\mathrm{dt} \approx 0.005$ pc cm^{-3} yr^{-1} over a six-year period.

Keith et al. (2013, see also You et al. (2007)) give $\mathrm{DM(t)}$ time series over ~ 6 yr for 20 millisecond pulsars that are monitored in the Parkes Pulsar Timing Array. Of these, 11 show prevailing trends of increasing DM (J1024−0719, J1730−2304, J1732−5049, and J1857+0943) or decreasing DM (J1045−4509, J1600−3053, J1643−1224, J1744−1134, J1909−3744, J1939+2134 and J2129−5721). Two others show overall trends but with a localized DM 'event' that breaks the trend (J1603−7202 and J1824−2452). The remaining seven objects show non-monotonic variations with various degrees and time scales of temporal correlation. The approximate derivative for J1939+2134 (B1937+21) is about half the value of the 20-yr trend reported by Ramachandran et al. (2006), and is consistent with changes in slope seen in the 20-yr time series.

Demorest et al. (2013) present $\mathrm{DM(t)}$ time series for 14 out of 17 pulsars that were timed. Of these, the seven objects that overlap with the (Keith et al. 2013) sample show consistent trends. Several objects show very weak DM variation while two, B1855+09 and J2317+1439, show strong trends superposed with correlated variations.

Phillips & Wolszczan (1991) report results on five pulsars, four of which show long-term trends with slopes $|d\mathrm{DM}/\mathrm{dt}| \sim 10^{-3}$ pc cm^{-3} yr^{-1} (increasing: B0823+26, B0834+06, and B1237+25; decreasing: B0919+06). They assert that the rms DM variations are correlated with the average DM but with significant scatter about a best fit relation $\sigma_{\mathrm{DM}} \propto \mathrm{DM}^{1.3\pm0.3}$. A trend of this type would generally signify that the DM variations are associated with accumulated effects along the line of sight, but the correlation is affected by the long-term trends that may be due to parallel motion through ionized gas near the pulsars.

Are the long terms trends seen in more than half of the pulsars due predominantly to parallel or transverse motion?

B1534+12: Fonseca et al. (2014) present $\mathrm{DM(t)}$ for the relativistic binary B1534+12 and fit for derivatives $d\mathrm{DM}/\mathrm{dt}$ in five separate time blocks. The overall trend is a decrease with time that is interrupted by episodic flattenings or increases in DM. The time series is remarkably similar to those shown in Figure 6, suggesting that there are interleaved density structures along the LOS. Contemporaneous scintillation parameters and the pulsar's flux density would be valuable for testing whether the DM time series is at all contaminated by diffraction and refraction effects.

Some possible projects:

1. Analyze published DM time series to test the fraction of pulsars for which changing distances are mostly responsible. Increasing and decreasing trends should occur with equal probability, on average. Where possible, scintillation parameters and flux densities can be used to discern the role, if any, of diffraction and refraction.

2. Ditto for NANOGrav time series.

3. Numerical modeling of dispersion, refraction, and diffraction to help identify ISM structure shapes needed to account for cases where trends are not monotonic and where a pure stochastic process is an insufficient explanation.

4. Investigation of additional ISM tracers along pulsar LOS, including free-free and Hα emission, recombination lines, strong Faraday rotation, and optical absorption lines.

5. Modeling of the solar system's bow shock and heliosphere-ISM boundary to assess whether time-variable contributions to pulsar DMs are significant and at all correlated between different LOS.

3 Frequency Dependent Dispersion Measures from Phase-screen Averaging

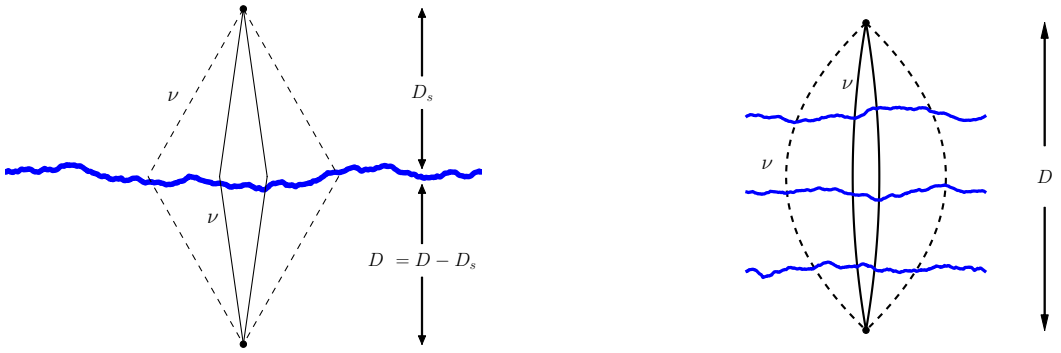

Figure 8: Scattering geometries for scattering from a thin screen (left) and filled medium (right). The pulsar-observer distance is D. Solid lines show ray paths at frequency ν that represent the characteristic width of the ray-path bundle and dashed lines are for frequency $\nu' < \nu$. The thin screen is at a distance D_s from the pulsar (p) and D' from the observer (o). For the filled medium the curved lines represent twice the rms ray-path deviation from the direct ray for a medium filled with statistically-homogeneous plasma variations. Three electron density slices are shown.

This section takes an approach where diffraction and refraction are both described by a wavenumber spectrum for electron density variations[2].

The following definitions are used here and in the next section. The pulsar-Earth distance is D, the pulsar-screen distance is D_s, and $D' = D - D_s$. Vectors transverse to the line of sight are $\mathbf{x_o}$ in the observer's plane, $\mathbf{x}$ in the screen plane, and $\mathbf{x_s}$ in the source plane. Figure 8 shows the geometry and schematic ray paths for frequencies ν and $\nu' < \nu$ for both a thin screen and with a thick medium.

The screen phase ϕ is related to the electron density by

$$\phi(\mathbf{x}) = -\lambda r_e \int_{\text{screen}} dz\, n_e(\mathbf{x}, z) \equiv -\lambda r_e N_e(\mathbf{x}), \tag{55}$$

where r_e is the classical electron radius and the second equation defines the column density $N_e(\mathbf{x})$. In this section we consider the electron density to have a wide range of scales described by a wavenumber spectrum $P_{\delta n_e}(\mathbf{q})$. The measured DM at a given frequency is related to how scattered rays that reach the observer sample the dispersing plasma. At low frequencies the sampled volume is larger so the column density will be different than at high frequencies.

Again, we analyze a thin screen for simplicity and define an averaging function $A_\nu(\mathbf{x})$ that has unit area, $\int d\mathbf{x}\, A_\nu(\mathbf{x}) = 1$. As in the previous section, a suitable averaging function is the normalized

[2]The calculation is very similar to the one in Appendix C of Cordes & Shannon (2010), but more explicitly compares the measureable DM values at two frequencies. The resulting scaling law is very similar but easier to interpret in this new approach.

scattered image. The scattering-averaged DM is

$$\overline{\mathrm{DM}}_\nu = \int d\mathbf{x}'\, A_\nu(\mathbf{x}') N_e(\mathbf{x}'). \tag{56}$$

The averaging function alters the time variations of DM. At high frequencies, the variations will generally be faster because the smoothing length is smaller but the amount of variation depends on the wavenumber spectrum.

We assume the electron density has the form of a local mean and a fluctuating part, $\bar{n}_e + \delta n_e(\mathbf{x})$. The mean contributes to the mean DM and is subtracted out in our analysis. For the fluctuating part, we use the power-law spectrum of Eq. **??** where the irregularities are isotropic. In this case, the the scattered image is symmetric.

We want to quantify the difference in DM between two frequencies, ν and ν'. The best statistic for this purpose is the mean-square difference (the structure function),

$$\begin{aligned} D_{\delta\mathrm{DM}}(\nu,\nu') &= \left\langle \left[\delta\overline{\mathrm{DM}}_\nu - \delta\overline{\mathrm{DM}}_{\nu'}\right]^2 \right\rangle \\ &= \left\langle (\delta\overline{\mathrm{DM}}_\nu)^2 \right\rangle + \left\langle (\delta\overline{\mathrm{DM}}_{\nu'})^2 \right\rangle - 2\left\langle \delta\overline{\mathrm{DM}}_\nu \delta\overline{\mathrm{DM}}_{\nu'} \right\rangle . \end{aligned} \tag{57}$$

The reasoning is as follows. The mean-square of $\overline{\mathrm{DM}}_\nu$ includes all of the power in the wavenumber spectrum from the lowest wavenumber q_0 to the wavenumber corresponding to the smoothing length, $q_s \approx 2\pi/D'\theta_{d\nu}$. The low wavenumbers will produce time variations in DM on very long time scales up to a million years or longer. We are concerned with much shorter time scales and wavenumbers that correspond to them.

Each of the three terms in Eq. 57 can be calculated from the DM cross correlation,

$$\begin{aligned} C_{\delta\overline{\mathrm{DM}}}(\nu,\nu') &= \left\langle \delta\overline{\mathrm{DM}}_\nu \delta\overline{\mathrm{DM}}_{\nu'} \right\rangle \\ &= \iint d\mathbf{x} d\mathbf{x}'\, A_\nu(\mathbf{x}') A_\nu(\mathbf{x}'') \iint dz' dz''\, \langle \delta n_e(\mathbf{x}', z) \delta n_e(\mathbf{x}'', z') \rangle. \end{aligned} \tag{58}$$

In general the electron-density correlation is

$$\langle \delta n_e(\mathbf{x}', z) \delta n_e(\mathbf{x}'', z') \rangle = \int d\mathbf{q}\, P_{\delta n_e}(\mathbf{q}) e^{i(\mathbf{q}_\perp \cdot (\mathbf{x}' - \mathbf{x}'') + q_z(z' - z''))}. \tag{59}$$

Thin screen geometry is invoked assuming that the screen thickness $\Delta z \gg q_0^{-1}$ and that $P_{\delta n_e}$ does not change with z, so that

$$\iint dz' dz''\, e^{i(q_z(z' - z''))} = \Delta z \delta(q_z). \tag{60}$$

Then

$$C_{\delta\overline{\mathrm{DM}}}(\nu,\nu') = \Delta z \iint d\mathbf{x} d\mathbf{x}'\, A_\nu(\mathbf{x}') A_\nu(\mathbf{x}'') \int d\mathbf{q}_\perp\, P_{\delta n_e}(\mathbf{q}_\perp) e^{i\mathbf{q}_\perp \cdot (\mathbf{x}' - \mathbf{x}'')}. \tag{61}$$

With a change of variables to $\overline{x} = (\mathbf{x}' + \mathbf{x}'')/2$ and $\delta\mathbf{x} = \mathbf{x}' - \mathbf{x}''$ for which $d\mathbf{x}'d\mathbf{x}'' = d\overline{x}d\delta\mathbf{x}$ and defining the cross-correlation

$$C_A(\delta\mathbf{x};\nu,\nu') = \int d\delta\mathbf{x}\, A_\nu(\overline{x}+\delta\mathbf{x}/2)A_{\nu'}(\overline{x}-\delta\mathbf{x}/2), \tag{62}$$

Eq. 61 becomes

$$C_{\delta\overline{\mathrm{DM}}}(\nu,\nu') = \Delta z \int d\mathbf{q}_\perp\, P_{\delta n_e}(\mathbf{q}_\perp) \int d\delta\mathbf{x}\, e^{i\mathbf{q}_\perp\cdot\delta\mathbf{x}} C_A(\delta\mathbf{x};\nu,\nu'). \tag{63}$$

Recognizing the second integral as the Fourier transform of C_A,

$$\widetilde{C}_A(\mathbf{q}_\perp;\nu,\nu') = \int d\mathbf{y}\, e^{i\mathbf{q}_\perp\cdot\mathbf{y}} C_A(\mathbf{y};\nu,\nu'), \tag{64}$$

we have

$$C_{\delta\overline{\mathrm{DM}}}(\nu,\nu') = \Delta z \int d\mathbf{q}_\perp\, P_{\delta n_e}(\mathbf{q}_\perp)\widetilde{C}_A(\mathbf{q}_\perp;\nu,\nu'). \tag{65}$$

The effect of the smoothing function is to limit the range of wavenumbers contributing to the DM cross correlation.

Now, using the DM cross correlation we can evaluate the structure function defined in Eq. 57,

$$\begin{aligned} D_{\delta\overline{\mathrm{DM}}}(\nu,\nu') &= \left\langle(\delta\overline{\mathrm{DM}}_\nu)^2\right\rangle + \left\langle(\delta\overline{\mathrm{DM}}_{\nu'})^2\right\rangle - 2\left\langle\delta\overline{\mathrm{DM}}_\nu\delta\overline{\mathrm{DM}}_{\nu'}\right\rangle \\ &= C_{\delta\overline{\mathrm{DM}}}(\nu,\nu) + C_{\delta\overline{\mathrm{DM}}}(\nu',\nu') - 2C_{\delta\overline{\mathrm{DM}}}(\nu,\nu') \\ &= \Delta z \int d\mathbf{q}_\perp\, P_{\delta n_e}(\mathbf{q}_\perp)\left[\widetilde{C}_A(\mathbf{q}_\perp;\nu,\nu) + \widetilde{C}_A(\mathbf{q}_\perp;\nu',\nu') - 2\widetilde{C}_A(\mathbf{q}_\perp;\nu,\nu')\right]. \end{aligned} \tag{66}$$

3.1 Estimate for a Power-law Wavenumber Spectrum

To get an estimate for the two-frequency DM cross correlation, a circularly symmetric Gaussian function is assumed for the smoothing function $A_\nu(\mathbf{x})$,

$$A_\nu(\mathbf{x}) = (2\pi\sigma_\nu^2)^{-1} e^{-x^2/2\sigma_\nu^2}. \tag{67}$$

The two-frequency cross correlation of $A_\nu(\mathbf{x})$ is

$$C_A(\delta\mathbf{x};\nu,\nu') = \left[2\pi(\sigma_\nu^2 + \sigma_{\nu'}^2)\right]^{-1} e^{-(\delta x)^2/2(\sigma_\nu^2+\sigma_{\nu'}^2)} \tag{68}$$

and its Fourier transform is

$$\widetilde{C}_A(\mathbf{q}_\perp;\nu,\nu') = e^{-{q_\perp}^2(\sigma_\nu^2+\sigma_{\nu'}^2)/2}. \tag{69}$$

The DM cross correlation is then

$$D_{\delta\overline{\mathrm{DM}}}(\nu,\nu') = \Delta z \int d\mathbf{q}_\perp\, P_{\delta n_e}(\mathbf{q}_\perp)\left[e^{-(q_\perp\sigma_\nu)^2} + e^{-(q_\perp\sigma_{\nu'})^2} - 2e^{-{q_\perp}^2(\sigma_\nu^2+\sigma_{\nu'}^2)/2}\right]. \tag{70}$$

Recognize σ_ν^{-1}, $\sigma_{\nu'}^{-1}$, and $\sqrt{2}(\sigma_\nu^2 + \sigma_{\nu'}^2)^{-1/2}$ as the approximate cutoffs in the integrals for each of the three terms.

Now we adopt the power-law wavenumber spectrum of Eq. 33 whose dependence on only the magnitude of the wavenumber is consist with the assumed symmetry of the smoothing function. Assuming the approximate cutoffs from the smoothing functions are all between q_0 and q_1, each term yields

$$\int_{q_0}^{q_c} d\mathbf{q}_\perp \; P_{\delta n_e}(\mathbf{q}_\perp) = 2\pi \mathrm{C_n^2} \int_{\mathrm{q_0}}^{\mathrm{q_c}} \mathrm{dq_\perp} \; {\mathrm{q_\perp}}^{1-\beta} = \frac{2\pi \mathrm{C_n^2}}{\beta - 2} \left(\mathrm{q_0^{2-\beta}} - \mathrm{q_c^{2-\beta}} \right). \tag{71}$$

The integral is dominated by the term involving $q_0 \ll q_c$ for $\beta > 2$ but in the expression for $D_{\delta\overline{\mathrm{DM}}}(\nu, \nu')$, the three terms involving q_0 cancel.

Defining the screen scattering measure as $\mathrm{SM} = \Delta \mathrm{z} \mathrm{C_n^2}$, the two-frequency correlation is

$$D_{\delta\overline{\mathrm{DM}}}(\nu, \nu') = \frac{2\pi \mathrm{SM}}{\beta - 2} \left[2^{(4-\beta)/2} \left(\sigma_\nu^2 + \sigma_{\nu'}^2 \right)^{(\beta-2)/2} - \sigma_\nu^{\beta-2} - \sigma_{\nu'}^{\beta-2} \right]. \tag{72}$$

Further simplification can be made by recognizing that $\sigma_\nu = D' \theta_{d_\nu}$ is the length scale on the screen corresponding to the observed diffraction (or scattering) angle θ_{d_ν}. The scattering angle scales with frequency as $\theta_{d_\nu} \propto \nu^{-\beta/(\beta-2)}$. Using this frequency scaling and using ν as a reference frequency, the two-frequency DM correlation becomes

$$D_{\delta\overline{\mathrm{DM}}}(\nu, \nu') = \frac{2\pi \mathrm{SM}}{\beta - 2} \left(D' \theta_{d_\nu} \right)^{\beta-2} F_\beta(\nu/\nu'), \tag{73}$$

where the frequency scaling function $F_\beta(x)$ is defined as

$$F_\beta(x) = 2^{(4-\beta)/2} \left[1 + x^{2\beta/(\beta-2)} \right]^{(\beta-2)/2} - x^\beta - 1. \tag{74}$$

This function vanishes for $x = 1$ as expected.

For a Kolmogorov screen with $\beta = 11/3$,

$$D_{\delta\overline{\mathrm{DM}}}(\nu, \nu') = \frac{6\pi \mathrm{SM}}{5} \left(D' \theta_{d_\nu} \right)^{5/3} F_{11/3}(\nu/\nu'). \tag{75}$$

the scaling function is $F_{11/3}(2) = 1.115$ for a 2:1 frequency range such as $\nu = 1.6$ GHz and $\nu' = 0.8$ GHz. Figure 9 shows $F_\beta(x)$ for $1 \le x \le 5$. Eq. 73 is written assuming that the fiducial frequency is the larger frequency ($\nu \ge \nu'$), so that the function F_β is defined for arguments $x \ge 1$.

3.1.1 DM changes in terms of SM and scattering angle

Evaluating Eq. 73 using fiducial values $D' = 1$ kpc, $\theta_{d_\nu} = 1$ mas, and $\mathrm{SM} = 10^{-3.5}$ kpc m$^{-20/3}$ we obtain

$$D_{\delta\overline{\mathrm{DM}}}(\nu, \nu') = 3.5 \times 10^{-10} \; (\mathrm{pc \; cm^{-3}})^2 \left(\frac{\mathrm{SM}}{10^{-3.5} \; \mathrm{kpc \; m^{-20/3}}} \right) \left(D'_{\mathrm{kpc}} \theta_{d_\nu, \mathrm{mas}} \right)^{5/3} F_{11/3}(\nu/\nu'). \tag{76}$$

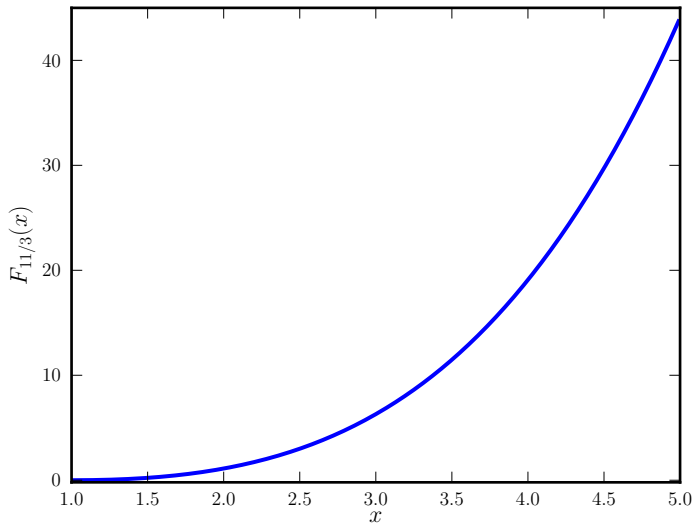

Figure 9: Plot of the frequency scaling function for a Kolmogorov spectrum $F_{11/3}(x)$.

Expressing this as a DM difference by taking the square root, we have

$$\delta\overline{\mathrm{DM}}(\nu/\nu') = 1.9\times10^{-5}\ (\mathrm{pc\ cm^{-3}})\left(\frac{\mathrm{SM}}{10^{-3.5}\ \mathrm{kpc\ m^{-20/3}}}\right)^{1/2}(D'_{\mathrm{kpc}}\theta_{d_\nu,\mathrm{mas}})^{5/6}\,F_{11/3}^{1/2}(\nu/\nu'). \quad (77)$$

We can evaluate the TOA difference associated with this difference in DM, but there is a dependence on the choice of frequency. Using the higher frequency ν (in GHz), the TOA difference is

$$\begin{aligned}\Delta t(\nu/\nu') &= 4.15\ \mathrm{ms}\ \nu^{-2}\delta\overline{\mathrm{DM}}(\nu/\nu') \\ &= 78\ \mathrm{ns}\left(\frac{\mathrm{SM}}{10^{-3.5}\ \mathrm{kpc\ m^{-20/3}}}\right)^{1/2}(D'_{\mathrm{kpc}}\theta_{d_\nu,\mathrm{mas}})^{5/6}\ \nu^{-2}F_{11/3}^{1/2}(\nu/\nu'). \quad (78)\end{aligned}$$

NB: the scattering angle θ_{d_ν} in these equations is the 'σ' of a Gaussian smoothing function. It would be better to use the FWHM; this replacement will be done in a future version.

3.1.2 $\delta\overline{\mathrm{DM}}$ in terms of SM only

The diffraction angle is not an independent quantity because it depends on $\mathrm{SM}\,\nu$, and the screen distance D_s. It can be found by setting the phase structure function at the observer's location equal to 2 rad^2, corresponding to the 1/e half-width of the visibility function, and relating the so-obtained length scale to the width of the scattered image (Coles et al. 1987, Eq. 1-8; Cordes & Rickett 1998, Appendix B). The full width at half maximum (FWHM) scattering diameter is given by

$$\theta_{d_\nu}(\mathrm{FWHM}) = \frac{2^{(\beta-3)/(\beta-2)}\sqrt{\ln 2}}{\pi}\left(\frac{\mathrm{D_s}}{\mathrm{D}}\right)\left(\mathrm{f_\beta r_e^2}\right)^{1/(\beta-2)}\lambda^{\beta)/(\beta-2)}\mathrm{SM}^{1/(\beta-2)} \quad (79)$$

where (Cordes & Rickett 1998; Eq. B6)

$$f_\beta = \frac{8\pi^2}{(\beta-2)2^{\beta-2}} \frac{\Gamma(2-\beta/2)}{\Gamma(\beta/2)}. \tag{80}$$

For a Kolmogorov medium $f_{11/3} = 88.3$ and the scattering diameter is

$$\theta_{d_\nu}(\mathrm{FWHM}) = 1.02 \text{ mas } \nu^{-11/5} \left(\frac{\mathrm{SM}}{10^{-3.5} \text{ kpc m}^{-20/3}} \right) \left(\frac{\mathrm{D_s}}{\mathrm{D}} \right). \tag{81}$$

Now, relating the FWHM to the one-sigma width of a Gaussian function,

$$\theta_{d_\nu}(\text{one sigma}) = \frac{\theta_{d_\nu}(\mathrm{FWHM})}{2\sqrt{2\ln 2}}, \tag{82}$$

we have from Eq. 73

$$D_{\delta\overline{\mathrm{DM}}}(\nu,\nu') = \frac{2\pi f_\beta c^\beta r_e^2}{(\beta-2)2^{\beta/2}} \left(\frac{D' D_s}{D} \right)^{\beta-2} \mathrm{SM}^2 \, \nu^{-\beta} \mathrm{F}_\beta(\nu/\nu'). \tag{83}$$

For a Kolmogorov medium we have

$$\begin{aligned} D_{\delta\overline{\mathrm{DM}}}(\nu,\nu') &= \frac{6\pi f_{11/3} c^{11/3} r_e^2}{5 \times 2^{11/6}} \left(\frac{D' D_s}{D} \right)^{5/3} \mathrm{SM}^2 \, \nu^{-11/3} \mathrm{F}_{11/3}(\nu/\nu') & (84) \\ &= 2.72 \times 10^{-10} \text{ (pc cm}^{-3})^2 \, \nu^{-11/3} F_{11/3} \left(\frac{\nu}{\nu'} \right) \\ &\quad \times \left(\frac{D'_{\mathrm{kpc}} D_s}{D} \right)^{5/3} \left(\frac{\mathrm{SM}}{10^{-3.5} \text{ kpc m}^{-20/3}} \right)^2. & (85) \end{aligned}$$

The rms difference is then

$$\delta\overline{\mathrm{DM}}(\nu,\nu') = 1.65 \times 10^{-5} \text{ (pc cm}^{-3}) \, \nu^{-11/6} F_{11/3}^{1/2} \left(\frac{\nu}{\nu'} \right) \left(\frac{D'_{\mathrm{kpc}} D_s}{D} \right)^{5/6} \left(\frac{\mathrm{SM}}{10^{-3.5} \text{ kpc m}^{-20/3}} \right) \tag{86}$$

and the arrival-time difference due to the DM difference evaluated at the higher frequency is

$$\begin{aligned} \Delta t_{\delta\overline{\mathrm{DM}}(\nu,\nu')}(\nu) &= 4.15 \text{ ms } \nu^{-2} \delta\overline{\mathrm{DM}}(\nu/\nu') \\ &= 69 \text{ ns } \nu^{-23/6} F_{11/3}^{1/2} \left(\frac{\nu}{\nu'} \right) \left(\frac{D'_{\mathrm{kpc}} D_s}{D} \right)^{5/6} \left(\frac{\mathrm{SM}}{10^{-3.5} \text{ kpc m}^{-20/3}} \right). & (87) \end{aligned}$$

3.1.3 Interpretation and Caveat

The difference $\delta\overline{\mathrm{DM}}(\nu,\nu')$ grows with increasing ratio ν/ν' (for fixed ν) because the scattering-averaged $\overline{\mathrm{DM}}_{\nu'}$ random walks away from the value at frequency ν. The growth of the DM difference is contained in $F_\beta^{1/2}(\nu/\nu')$.

The arrival-time difference $\Delta t_{\overline{\delta \mathrm{DM}}(\nu,\nu')}(\nu)$ is the deviation from the normal DM delay at frequency ν associated with the DM difference $\overline{\mathrm{DM}}(\nu,\nu')$. The deviation at the lower frequency ν' is a factor ν^2/ν'^2 larger. In other words, if the TOA and DM are both measured at frequency ν', an extrapolation of the TOA to frequency ν would show a timing offset compared to the TOA actually measured at frequency ν. This offset is equal to $\Delta t_{\overline{\delta \mathrm{DM}}(\nu,\nu')}(\nu)$. Restated again, the pulses at frequency ν trace a dispersion trajectory that is slightly different from the trajectory at frequency ν'.

The calculation undertaken here simply looks at the difference in electron column density that results from how the ray-path bundle that samples the screen changes with frequency. The calculation of the arrival-time difference therefore does not take into account additional delays that result from the ray-path bundle shifting laterally (due to refraction) or changing shape, due to focusing and defocusing from the screen. These additional effects are analyzed using the second approach in §4.

3.2 Suggested Studies

Results in the literature already suggest that DM values are discrepant for a few pulsars when different frequency bands or pairs of frequencies are used to estimate them. However, it is not clear that these are really 'frequency-dependent DMs' or instead the result of intrinsic variation of pulse profiles with frequency. Detailed studies of a few pulsars using simultaneous observations with wide frequency coverage need to be done where profile evolution and DM variations are both taken into account. Assuming profile evolution is epoch-independent will help disentangling the various effects, but intrinsic mode changes and changing pulse broadening from multipath propagation may add uncertainty to the analysis.

4 Effects of Refraction on Scattering, Scintillation, and Timing

The starting point is the Kirchoff diffraction integral (KDI) that we write in the form

$$\varepsilon(\mathbf{x_o}, t, \nu, \mathbf{x}_s) = (i\lambda D_s)^{-1} \int d\mathbf{x}'\, e^{i\Psi(\mathbf{x_o}, t, \nu, \mathbf{x}, \mathbf{x_s})} \tag{88}$$

$$\Psi(\mathbf{x_o}, t, \nu, \mathbf{x}, \mathbf{x_s}) = \phi_g(\mathbf{x_o}, \mathbf{x}, \mathbf{x_s}) + \phi_r(\mathbf{x}) + \phi_d(\mathbf{x}). \tag{89}$$

Here ϕ_g is the geometric 'kernel' for the KDI,

$$\phi_g(\mathbf{x_o}, \mathbf{x}, \mathbf{x_s}) = \frac{\pi}{\lambda}\left(D_s^{-1}|\mathbf{x}-\mathbf{x_s}|^2 + D'^{-1}|\mathbf{x_o}-\mathbf{x}|^2 - D^{-1}|\mathbf{x_o}-\mathbf{x_s}|^2\right). \tag{90}$$

In the following, we consider the observer and source to be on axis with $\mathbf{x_o} = \mathbf{x_s} = \mathbf{0}$ that yields

$$\phi_g(\mathbf{x}) = \alpha\nu x^2 \tag{91}$$

$$\alpha = \frac{\pi}{c}\frac{D}{D_s D'}. \tag{92}$$

The diffraction phase is ϕ_d. The refraction phase is written as a quadratic expansion about the stationary-phase point (SPP) $\overline{\mathbf{x}}$ given by $\partial_{\mathbf{x}}[\phi_g(\mathbf{x_o}, \mathbf{x}, \mathbf{x_s}) + \phi_r(\mathbf{x})] = \mathbf{0}$,

$$\phi_r(\mathbf{x}) = a + \boldsymbol{b}\cdot(\mathbf{x}-\overline{\mathbf{x}}) + \frac{1}{2}(\mathbf{x}-\overline{\mathbf{x}})^\dagger \mathbf{C}(\mathbf{x}-\overline{\mathbf{x}}) \tag{93}$$

and where $\overline{\mathbf{x}}$ and $\boldsymbol{b}$ are related as

$$\boldsymbol{b} = -2\alpha\nu\overline{\mathbf{x}} \tag{94}$$

for the quadratic phase model. As required, the total phase is quadratic about the SPP,

$$\phi(\mathbf{x}) = \phi_g(\mathbf{x}) + \phi_r(\mathbf{x}) = a + \alpha\nu|\mathbf{x} - \overline{\mathbf{x}}|^2 + \frac{1}{2}(\mathbf{x} - \overline{\mathbf{x}})^\dagger \mathbf{C}(\mathbf{x} - \overline{\mathbf{x}}). \tag{95}$$

More generally, the refraction phase could have multiple SPPs and an expansion would be needed around each.

The diffraction phase determines the scattered image shape in the absence of refraction. The scattered image is the Fourier transform of the visibility function $\Gamma_\varepsilon(\delta\mathbf{r})$ given by the phase structure function $D_\phi(\delta\mathbf{r})$,

$$\Gamma_\varepsilon(\delta\mathbf{r}) \equiv \langle \varepsilon(\mathbf{x}, t, \nu, \mathbf{x}_s)\varepsilon^*(\mathbf{x} + \delta\mathbf{r}, t, \nu, \mathbf{x}_s)\rangle = e^{-\frac{1}{2}D_\phi(\delta\mathbf{r})} \tag{96}$$

$$D_\phi(\delta\mathbf{r}) = \left\langle [\phi_d(\mathbf{x}) - \phi_d(\mathbf{x} + \delta\mathbf{r})]^2 \right\rangle. \tag{97}$$

The Fourier transform of the visibility function gives the image (with subscript '0' to denote no refraction),

$$I_0(\boldsymbol{\theta}) = \int d\delta\mathbf{r}\, e^{i\boldsymbol{\theta}\delta\mathbf{r}} \Gamma_\varepsilon(\delta\mathbf{r}). \tag{98}$$

Let the unrefracted image have a mean-square scattering angle

$$\langle|\boldsymbol{\theta}|^2\rangle_0 = \frac{\int d\boldsymbol{\theta}\, |\boldsymbol{\theta}|^2 I_0(\boldsymbol{\theta})}{\int d\boldsymbol{\theta}\, I_0(\boldsymbol{\theta})} \equiv \sigma_0^2. \tag{99}$$

Refraction alters the image, flux density, arrival time, pulse broadening, and scintillation parameters. For simplicity, results are given for the case where the scattered image $I_0(\theta)$ is circularly symmetric when there is no refraction. We also assume, for simplicity, that ellipses of constant refraction phase in Eq. 93 align with the transverse coordinate axes (x, y). In this case, $\mathbf{C}$, is diagonal with elements $C_{x,y}$

A more general treatment would relax both of these assumptions because there is evidence for diffraction to be asymmetric and because the refraction phase derives from a stochastic process, the matrix $\mathbf{C}$ will generally not be diagonal. However our goal here is to develop expressions for the simplest case.

4.1 Image and Flux Density

By consolidating linear and quadratic terms, the refraction-distorted image becomes

$$I(\boldsymbol{\theta}) = I_0(G_x^{-1}(\theta_x - \overline{\theta}_x), G_y^{-1}(\theta_y - \overline{\theta}_y)), \tag{100}$$

where the image centroid is

$$\overline{\boldsymbol{\theta}} = \frac{\overline{\mathbf{x}}}{D'} \tag{101}$$

and the gains are given by (with $k = 2\pi/\lambda$)

$$G_{x,y} = \left[1 + \frac{D_s D' C_{x,y}}{kD}\right]^{-1}. \tag{102}$$

Gains $G_{x,y} > 1$ imply that the image is wider in the x, y directions compared to the unity gain case. While the amplitude of the image is unaltered, the integral over the image is altered by a factor $G_x G_y$, so the flux density F_0 without refraction becomes

$$F = G_x G_y F_0 \tag{103}$$

4.2 Mean-Square Scattering Angle

We have

$$\langle |\boldsymbol{\theta}|^2 \rangle = \overline{\theta}^2 + \frac{1}{2}\left(G_x^2 + G_y^2\right)\sigma_0^2. \tag{104}$$

The first term is from the offset of the image from the direct ray path while the mean-square angular broadening of a point source is given by the second term.

4.3 Mean Time Delay

The group delay is given by $2\pi\tau_\nu = \partial_\nu\left[\phi_g + \phi_r\right]$ and we note that $\phi_g \propto \nu$ and $\phi_r \propto \nu^{-1}$. The group delay is a combination of the dispersion delay, the delay associated with the offset of the scattered image from the direct line of sight by refraction, and the scattering delay.

We average the delay over the scattered and refracted image to obtain

$$2\pi\langle\tau_\nu\rangle = -\nu a + \frac{\pi D D'}{c D_s}\left[\overline{\theta}^2 + \frac{1}{2}\left(G_x^2 + G_y^2\right)\sigma_0^2\right]. \tag{105}$$

The first term gives the dispersion delay $\propto \nu^{-2}$, the second is the geometric delay $\propto \nu^{-4}$ from the image centroid, and the third term is the scattering delay altered by wavefront curvature, so we write

$$\tau_\nu = \tau_{\mathrm{DM}_\nu} + \tau_{g_\nu} + \tau_{d_\nu}. \tag{106}$$

The pulse-broadening delay is

$$\tau_{d_\nu} = \frac{\pi D D'}{2 c D_s}\left(G_x^2 + G_y^2\right)\sigma_0^2. \tag{107}$$

In the absence of phase curvature, $\tau_{d_\nu} \propto \nu^{-4}$. However, the gains $G_{x,y}$ are frequency dependent. For small deviations from unit gain, $|G_{x,y} - 1| \ll 1$, we can write

$$G_{x,y}^2 \approx 1 - \frac{c D_s D'}{\pi D}\frac{C_{x,y}}{\nu}. \tag{108}$$

Since $C_{x,y} \propto \nu^{-1}$, it is clear that the pulse-broadening delay has a term with the conventional scaling $\propto \nu^{-4}$ along with a term that scales as ν^{-6} in this regime.

4.4 Scintillation Bandwidth

The scintillation bandwidth can be written in terms of the pulse broadening time as

$$\Delta\nu_d = \frac{C_1}{2\pi\tau_{d_\nu}} \tag{109}$$

where $C_1 \approx 1$ is a constant that depends on the wavenumber spectrum of the electron density variations and on the location of the scattering screen along the line of sight (and, more generally, on the thickness of the screen or medium).

The scintillation bandwidth with refraction is related to the value without refraction, $\Delta\nu_{d0}$, by

$$\Delta\nu_d = \frac{\Delta\nu_{d0}}{G_x^2 + G_y^2}. \tag{110}$$

4.5 Scintillation Time Scale

The scintillation time scale Δt_d can be derived from the phase structure function by solving

$$D_\phi(\mathbf{V}_{\rm eff}\Delta t_d) = 1, \tag{111}$$

where the effective velocity includes the transverse components of the individual velocities of the pulsar, the observer, and the medium (the screen),

$$\mathbf{V}_{\rm eff} = D'\mathbf{V}_{\rm p} + \frac{D_s}{D}\mathbf{V}_{\rm obs} - \mathbf{V}_{\rm m}. \tag{112}$$

The gains $G_{x,y}$ alter the image's width so they also change the contours of constant mean-square phase given by the structure function. If D_{ϕ_0} is the phase structure function when there is no refraction, we generally have

$$D_{\phi_0}\left(\sqrt{(G_x \mathrm{V}_{\mathrm{eff}_x})^2 + (G_y \mathrm{V}_{\mathrm{eff}_y})^2}\Delta t_d\right) = 1. \tag{113}$$

Then the refracted scintillation time is

$$\Delta t_d = \frac{\mathrm{V}_{\rm eff}\Delta t_{d_0}}{\sqrt{(G_x \mathrm{V}_{\mathrm{eff}_x})^2 + (G_y \mathrm{V}_{\mathrm{eff}_y})^2}}. \tag{114}$$

4.6 Scaling to Different Frequencies

The results in §§4.1 - 4.5 refer to quantities at a particular radio frequency ν. In particular, the expansions in Eq. 93-95 about a stationary-phase point are specific to the frequency ν. It is straightforward to generalize the results to an arbitrary frequency because the geometric phase $\phi_g \propto \nu$ while the refraction and diffraction phases scale as ν^{-1}. To do so we give subscripts to the SPP location $\overline{\mathbf{x}}_\nu$ and the expansion quantities a_ν, $\boldsymbol{b}_\nu$, and $\mathbf{C}_\nu$ defined previously. Then the phase-screen expansion in Eq. 93 becomes

$$\phi_{r_\nu}(\mathbf{x}) = a_\nu + \boldsymbol{b}_\nu \cdot (\mathbf{x} - \overline{\mathbf{x}}_\nu) + \frac{1}{2}(\mathbf{x} - \overline{\mathbf{x}}_\nu)^\dagger \mathbf{C}_\nu (\mathbf{x} - \overline{\mathbf{x}}_\nu). \tag{115}$$

At another frequency ν' we have the equivalent expansion

$$\phi_{r\nu'}(\mathbf{x}) = a_{\nu'} + \boldsymbol{b}_{\nu'} \cdot (\mathbf{x} - \overline{\mathbf{x}}_{\nu'}) + \frac{1}{2}(\mathbf{x} - \overline{\mathbf{x}}_{\nu'})^{\dagger}\mathbf{C}_{\nu'}(\mathbf{x} - \overline{\mathbf{x}}_{\nu'}), \tag{116}$$

where the expansion quantities at ν' are related to those at ν as

$$\begin{aligned} a_{\nu'} &= (\nu/\nu')[a_{\nu} + \boldsymbol{b}_{\nu} \cdot (\overline{\mathbf{x}}_{\nu'} - \overline{\mathbf{x}}_{\nu}) + \frac{1}{2}(\overline{\mathbf{x}}_{\nu'} - \overline{\mathbf{x}}_{\nu})^{\dagger}\mathbf{C}_{\nu}(\overline{\mathbf{x}}_{\nu'} - \overline{\mathbf{x}}_{\nu})] & (117)\\ \boldsymbol{b}_{\nu'} &= (\nu/\nu')\left[\boldsymbol{b}_{\nu} + \mathbf{C}_{\nu}(\overline{\mathbf{x}}_{\nu'} - \overline{\mathbf{x}}_{\nu})\right] & (118)\\ \mathbf{C}_{\nu'} &= \mathbf{C}_{\nu}. & (119) \end{aligned}$$

The location of the SPP scales as

$$\overline{\mathbf{x}}_{\nu} = (\nu/\nu')\mathbf{H}^{-1}(\nu')\mathbf{H}(\nu)\mathbf{x}_{\nu}, \tag{120}$$

where, using the 2×2 identify matrix $\mathbf{I}$,

$$\mathbf{H}(\nu) = 2\alpha\nu\mathbf{I} + (\nu/\nu')\mathbf{C}_{\nu} \tag{121}$$

A change in frequency from ν to ν' therefore changes the dispersion measure from $\mathrm{DM}_{\nu} = -\mathrm{a}_{\nu}/\nu$ to $\mathrm{DM}_{\nu'} = \mathrm{a}_{\nu'}/\nu'$. Other quantities also vary according to standard scaling laws for the unrefracted scattering parameters that are modified by the frequency-dependent refraction.

4.7 Summary of Dispersion and Refraction Effects

1. Dispersion measure: $\mathrm{DM} = -\mathrm{a}_{\nu}/\nu$ is determined by the screen phase a_{ν} at the stationary-phase point, $\overline{\mathbf{x}}$. DM is therefore frequency dependent because the SPP shifts with a change in frequency, causing a_{ν} to change in accordance with the quadratic phase model;
2. Image distortion: a circular image becomes elliptical image with axial ratio G_x/G_y;
3. Flux variation $\propto G_x G_y$;
4. Mean image location $\overline{\boldsymbol{\theta}} = \overline{\mathbf{x}}/D' = -(c/2\pi\nu)(D_s/D)\boldsymbol{b} \propto \nu^{-2}$;
5. Mean-square image size $\propto \left(G_x^2 + G_y^2\right)$;
6. Mean pulse-broadening time $\propto \left(G_x^2 + G_y^2\right)$;
7. Scintillation bandwidth $\propto \left(G_x^2 + G_y^2\right)^{-1}$;
8. Scintillation time scale $\propto \left[(G_x \mathrm{V}_{\mathrm{eff}_x})^2 + (G_y \mathrm{V}_{\mathrm{eff}_y})^2\right]^{-1/2}$.

If there is variation in the apparent flux density due to refraction, all other measureable quantities will also vary with epoch. If only linear refraction occurs, the image centroid and delay associated with it will be epoch dependent but none of the quantities involving $G_{x,y}$ will vary.

4.8 Utility and Suggested Studies

The use of a quadratic phase function to describe refraction and to renormalize the KDI leads to expressions that are useful in both simulations and for interpreting time series of flux densities, DM, and scintillation parameters.

Simulations: Calculation of the time dependence of DM for different frequencies can be streamlined by quadratically expanding the refraction phase around the SPP at an initial frequency and then calculating expansion parameters at other frequencies using expressions in §4.6. From these, differences in all measureable quantities can be calculated at different frequencies.

Data interpretation: The flux density, DM, and scintillation parameters have time dependences that are intertwined according to the summary expressions given above. Analysis of multi-epoch measurements can aim to demonstrate consistency. For example, if flux density variations are seen that can be attributed to refractive interstellar scintillations (RISS), then variations in DM, the scintillation parameters[3], and arrival time are expected. While it may not be possible to fully disentangle the refraction-screen parameters and predict variations in one quantity (e.g. scintillation time scale) from another (e.g. the flux density or the scintillation bandwidth), the variance and time scales of the different quantities should be consistent. Particularly valuable would be estimates of timing variations from measured variations of flux density and scintillation parameters. These can be used for timing noise-budget analyses and for optimizing observing programs with respect to frequency ranges and cadence, etc.

4.9 Time Variations of DM from a Thin Screen

Motions of the pulsar, observer, and screen will cause DM to be time dependent. As long as the pulsar is not embedded in the screen, only the transverse components of the velocity are relevant and the combine into the effective velocity given by Eq. 112. At a given frequency ν, the screen is sampled at a location $\mathbf{x}(t) = \overline{\mathbf{x}} + \mathbf{V}_{\rm eff} t$. The dispersion measure is then **Need to check this vis a vis total phase vs. just the refraction phase.**

$$\mathrm{DM(t)} = -\nu^{-1}\phi_{\rm r}(\mathbf{x}) = \nu^{-1}\left(\mathrm{a} + \boldsymbol{b}\cdot\mathbf{V}_{\rm eff}\mathrm{t} + \mathbf{V}_{\rm eff}{}^{\dagger}\mathbf{C}\mathbf{V}_{\rm eff}\mathrm{t}^2\right). \tag{122}$$

[3]Changes in the secondary spectrum and scintillation arcs should also occur.

References

Backer, D. C. et al. 1993, Ap. J., 404, 636

Clegg, A. W., Fey, A. L., & Lazio, T. J. W. 1998, Ap. J., 496, 253

Cognard, I., & Lestrade, J.-F. 1997, Ast. Ap., 323, 211

Cordes, J. M., Wolszczan, A., Dewey, R. J., Blaskiewicz, M., & Stinebring, D. R. 1990, Ap. J., 349, 245

Cordes, J. M. & Rickett, B. J. Ap. J., 507, 846

Demorest, P. B., Ferdman, R. D., Gonzalez, M. E., et al. 2013, Ap. J., 762, 94

Fonseca, E., Stairs, I. H., & Thorsett, S. E. 2014, Ap. J., 787, 82

Foster, R. S., & Cordes, J. M. 1990, Ap. J., 364, 123

Frisch, P. C. 2007, SINS - Small Ionized and Neutral Structures in the Diffuse Interstellar Medium, 365, 227

Gibson, S. J. 2007, SINS - Small Ionized and Neutral Structures in the Diffuse Interstellar Medium, 365, 59

Ilyasov, Y. P., Imae, M., Hanado, Y., et al. 2005, Astronomy Letters, 31, 30

Keith, M. J., Coles, W., Shannon, R. M., et al. 2013, MNRAS, 429, 2161

Löhmer, O. et al. 2001, Ap. J. Letters, 562, L157

Löhmer, O. et al. 2004, Ast. Ap., 425, 569

Maitia, V., Lestrade, J.-F., & Cognard, I. 2003, Ap. J., 582, 972

McClure-Griffiths, N. M., Dickey, J. M., Gaensler, B. M., Green, A. J., & Haverkorn, M. 2007, SINS - Small Ionized and Neutral Structures in the Diffuse Interstellar Medium, 365, 65

Phillips, J. A., & Wolszczan, A. 1991, Ap. J. Letters, 382, L27

Ramachandran, R., Demorest, P., Backer, D. C., Cognard, I., & Lommen, A. 2006, Ap. J., 645, 303

Rickett, B. J. 1990, Ann. Rev. Ast. Ap., 28, 56

Stanimirović, S., Heiles, C., & Kanekar, N. 2007, SINS - Small Ionized and Neutral Structures in the Diffuse Interstellar Medium, 365, 22

Stinebring, D. 2007, SINS - Small Ionized and Neutral Structures in the Diffuse Interstellar Medium, 365, 254

You, X. P., et al. 2007, MNRAS, 378, 493